Multi-channel near-infrared spectroscopy imaging system for improvement of diagnostic accuracy in localized prostate cancer

Seung-seob Kim

Department of Medicine
The Graduate School, Yonsei University

Multi-channel near-infrared spectroscopy imaging system for improvement of diagnostic accuracy in localized prostate cancer

Directed by Professor Dae Chul Jung

The Master's Thesis
submitted to the Department of Medicine,
the Graduate School of Yonsei University
in partial fulfillment of the requirements for the
degree of Master of Medical Science

Seung-seob Kim

June 2014

This certifies that the Master's Thesis

of Seung-seob Kim is approved.

Dae Chul Jung

Thesis Supervisor : Dae Chul Jung

Thesis Committee Member#1 : Young Taik Oh

Thesis Committee Member#2 : Koon Ho Rha

The Graduate School

Yonsei University

June 2014

Acknowledgements

이 논문은 2012-2014년도 정부(미래창조과학부)의 재원으로 한국연구재단의 지원을 받아 수행된 기초연구사업임(No. NRF-2012R1A1A1042668).

우선 부족한 저를 여기까지 이끌어 주신 정대철 교수님께 진심으로 깊은 감사 드립니다. 훌륭한 NIRS system을 개발해 주신 고려대학교 김법민 교수님, 최고의 광학 팬텀을 제작해 주신 GIST 김재관 교수님께도 깊은 감사 드립니다. 보다 나은 학위 논문이 되도록 조언을 아끼지 않아주셨던 오영택 교수님, 나군호 교수님, 정말 감사합니다. 그외 매일매일 제게 큰 가르침을 베푸시는 모든 세브란스 영상의학과 교수님들께도 진심으로 감사드립니다.

광학에 무지한 저를 끈기와 정성으로 계몽시켜준 송현아 씨, 완전 고맙습니다. 롤 만렙 달성도 축하드려요! 함께 도와주신 고달권 선생님과 백승호 선생님, 감사합니다. 현아 씨와 함께 GIST 출장 갔을 때 친절

하게 팬텀 제작법 전수해주시고 막걸리 같이 마셨던 이송현 선생님, 예브기니, 정말 고맙습니다.

함께 밤새며 같이 실험 도와준 의국의 보배 승수, 우리 JDC 연구실 랩장 명완이, 포레버 동물 사랑 웅희 씨, 모두 감사합니다.

그 외 직접적으로 이 논문에 도움을 준 바는 **전혀** 없지만 김승섭의 인생에 큰 고마움을 준 모든 사람들, such as 우리 영상의학과 의국 동기들 (손범석민, 장수, 승봉, 고지봉, 한더, 이미눅), 우리 의국 선/후배 선생님들 (특히 목동 사시는 안찬식 형님), 전설의 Korean nu metal band 텔레좀비 멤버들 (보컬 김thedarkness현석, 변태 드러머 영일, 디씨충 베이스 낙현, 페북 중독 기타 태준오빠, 윤아와 악수한 DJ 정헌), 좀비만세 멤버들 (낚이기 위해 태어난 빵소, 마약하는 싸패 힉, 메탈 여선생 최고야, 위대한 탄생 형우), 함께 Symphony X를 카피하며 최고의 European style power progressive melodic metal band 결성을 꿈꾸고 있는 멤버들 (보컬 김ㅈ키, 베이스 낙현, 드

럼 시환, 키보드 믿음), 연세의대 04학번 동기들 (큰 인물 승우형, 어린 영혼 배생, Jaguar 타는 남자 문생, 항암제 덕후 충근, 스미골 민씨, 부천 카사노바 영제형, 야동왕 김정호), 연세의대 선/후배님들 (연구 덕후 장지석 형님, 전설의 용사마, 마스터 요다 상수, 중2병 순행), 나의 중딩/목동 패밀리들 (홀든 파수꾼 현우, 글로발 휴머니스트 원재, 윈도우 덕후 진섭, 캡틴 상혁, 참치, 솬, 조마, 제스, 남스타, 그리고 연락두절 재준이), 열심히 사는 한의사 동생 영기, 나를 닮은 연예인들 (공유, 장기하), 위대한 musicians (Rhapsody of Fire, Luca Turilli's Rhapsody, Dream Theater, Symphony X, King Diamond, Yngwie Malmsteen, Tony Macalpine, Vitalij Kuprij, Shadow Gallery, Adagio, Marty Friedman, Jason Becker, Andy Timmons, Greg Howe, Eric Johnson, Joe Satriani, Steve Vai, Illusion Suite, DGM, Pagan's Mind, Withem, Graveworm, Dark Moor, Dark Tranquility, Kamelot, Labyrinth, Triosphere, Nightwish, Cradle of Filth, etc..), 모두 감사합니다.

마지막으로 저를 낳아주시고 길러주신 부모님, 사랑하는 할머니, 나의 영원한 팬 김보영, 그리고 세상에서 가장 사랑스러운 소연이, 모두 진심으로 감사드립니다.

<TABLE OF CONTENTS>

LIST OF FIGURES

LIST OF TABLES

Abstract

Multi-channel near-infrared spectroscopy imaging system for improvement of diagnostic accuracy in localized prostate cancer

Seung-seob Kim

Department of Medicine
The Graduate School, Yonsei University

(Directed by Professor Dae Chul Jung)

Purpose: The purpose of this study was to develop a multi-channel NIRS (near-infrared spectroscopy) system for improvement of diagnostic accuracy in localized prostate cancer and to verify its diagnostic capability with the optical phantoms of prostate cancer.

Materials and Methods: We developed the multi-channel NIRS system and the optical phantoms of normal prostate gland and localized prostate cancer. Computer software named Labview (National Instruments, Austin, TX, USA) was used to develop GUI (Graphic User Interface) which can process incoming signals and display them on the same monitor simultaneously. We measured NIRS signal attenuation through the developed phantoms and reconstructed 2D images based on the calculated absorption coefficients. We compared the reconstructed 2D images with the actual location of the localized prostate cancer component in the optical phantom.

Results: Area with high absorption coefficients was well correlated with the actual location of the localized prostate cancer component in the optical phantom.

Conclusion: We successfully demonstrated possibility of our NIRS system as a new potential imaging method for improvement of diagnostic accuracy in localized prostate cancer. In future, the NIRS system will possibly be combined with TRUS (trans-rectal ultrasonography), improving diagnostic accuracy of focal prostate cancer imaging and localization of target biopsy sites.

Key words : prostate cancer, NIRS, near-infrared spectroscopy, optical imaging, optics, NIRS-US, hybrid imaging

Multi-channel near-infrared spectroscopy imaging system for improvement of diagnostic accuracy in localized prostate cancer

Seung-seob Kim

Department of Medicine
The Graduate School, Yonsei University

(Directed by Professor Dae Chul Jung)

I. Introduction

1. NIRS (Near-infrared spectroscopy)

NIRS has been used in various scientific fields including not only biomedical field but also agriculture, chemical industry, life science, pharmaceutical, and textiles. Its major advantage is to test samples non-invasively and non-destructively [1]. Particularly in biomedical optics, its major application is a continuous and non-invasive monitoring of the tissue hemodynamics and oxidative metabolism [2].

In the forties, Glenn Millikan invented the muscle oximeter, the first medical device using the optical method [2,3]. In 1977, Frans Jöbsis was the first to report that the concentration of oxy-hemoglobin (HbO_2) and deoxy-hemoglobin (Hbr) in the brain tissue could be monitored continuously using his in vivo NIRS sytem [2,4,5].

NIRS is the optical method to measure changes in the concentration of chromophores, using light in the wavelengths between visible light and infrared. There exist many different kinds of chromophores in the human body. Water strongly absorbs light in the wavelengths below 300 nm and above

1000 nm, while light in the range between 400 and 650 nm is absorbed greatly by hemoglobin and melanin [6]. As a result, the wavelengths range of 700~900 nm, near-infrared (NIR), is the only optical window able to reach deep inside the human body [2,6,7]. Still some chromophores absorb NIR to some degree, and most of them are HbO_2 and Hbr in the microvessels with diameter less than 1 mm. Those in the large vessels are known to absorb NIR light completely [2]. Therefore attenuation of the NIRS signal mainly depends on the concentration of HbO_2 and Hbr in the small vessels [8]. Depth of NIRS penetration is known to be approximately one half of the source-detector distance [2]. Optical pathlength, the length of actual NIR light path inside the tissue, is always longer than the physical distance between the source and detector, as the light is influenced by complex scattering effects inside the different tissue layers [2].

There are three different NIRS techniques: Continuous wave, Frequency-domain, and Time-domain.

Continuous wave method is most commonly used among the three modalities and characterizes in constant tissue illumination. It measures only the light attenuation, which can be used to calculate the changes in the concentrations of HbO_2 and Hbr by modified Beer-Lambert law. The optical properties - scattering (μ_s') and absorption (μ_a) coefficients - cannot be determined, and thus neither the absolute concentrations of HbO_2 and Hbr. It is the cheapest method and easiest of transport [2,9].

The other two methods measure not only light attenuation but also time factor. Frequency-domain technique uses intensity-modulated light, measuring both the light attenuation and phase delay. Time-domain technique uses short pulses of light and measures the shape of the pulse. These two methods can offer the optical properties, from which the absolute concentrations of HbO_2 and Hbr can be calculated. They also have advantage of deeper penetration through the human tissues. However, frequency-domain

method is more expensive and bulky, and requires more complex technologies than continuous-wave technique, while time-domain technique is even more expensive, and needs far larger and more complicated system than frequency-domain modality [2,10]. Because of these reasons, time-domain method has been regarded as a failed approach in the biomedical field, supported by the fact that there is only one commercially available dual-channel time-domain NIRS system (TRS-20, Hamamatsu Photonics K.K., Japan) while most of commercial NIRS instruments are based on continuous wave technique [10].

2. Analysis of NIRS signal attenuation

Among the various algorithms to convert light attenuation into the concentrations of HbO_2 and Hbr, modified Beer-Lambert law is most commonly used [9,11]. It is based on several assumptions.

1) Investigated areas are assumed to be homogeneous.
2) μ_s' is much larger than μ_a.
3) μ_s' does not change with time
4) Chromophores other than HbO_2 and Hbr absorb NIR light minimal enough to be ignored.

The first assumption is not true as the human tissues are always heterogeneous, leading to the quantification errors. However, qualitative trend of concentration changes of chromophores is still generally correct. The other three assumptions are generally regarded to be true when it comes to the human tissues.

Through Beer-Lambert law was the first important discovery in terms of the quantification, it does not take into account light scattering [12,13]. Delpy [6] modified Beer-Lambert law to be used even in the media under light scattering effect. Modified Beer-Lambert law includes differential pathlength factor (DPF), which accounts for the increased distance of travelling light caused by μ_s'. As DPF can be measured only by time-domain technique,

review of previous studies which already measured DPF within each part of the human body is needed when using continuous wave method. The modified Beer-Lambert law is defined as follows:

$$\Delta OD^{\lambda} = -ln\frac{I(t)}{I_0} = (\epsilon^{\lambda}_{HbO_2}\Delta[HbO_2] + \epsilon^{\lambda}_{Hbr}\Delta[Hbr])B^{\lambda}L$$

ΔOD^{λ}: optical density (light attenuation), I_0: intensity of initial light source, $I(t)$: change in intensity of light source according to time, ε^{λ}: extinction coefficient of HbO_2 and Hbr in the given wavelength, B^{λ}: DPF in the given wavelength, L: length between source and detector.

3. Prostate cancer

A. Epidemiology

In the United States, prostate cancer is the second most common male malignancy, after the skin cancer [14,15]. The estimated numbers of new cancer cases and cancer deaths from prostate cancer in 2013 were 238,590 and 29,720, respectively, each ranking first and second among male malignancies in the United States [16]. Likewise, the incidence of male prostate cancer in Korea is rapidly increasing with the annual percentage change between 1999 and 2010 of 12.8%, which is second to that of thyroid cancer of 24.8% [17].

There are several risk factors regarding the development of prostate cancer. Among them, age older than 40 years is generally accepted as the most significant factor [15,18]. Smoking history, family history of prostate cancer, low physical activity levels, high BMI (body mass index), tall height, and high intakes of calory, calcium, and alpha-linolenic acid have been also noted as significant risk factors of prostate cancer [19].

B. Prognosis

The prognosis of prostate cancer varies depending on its stage. According to American Cancer Society, 5-year survival rate of local and regional stages is 100%, while that of distant stage is as low as 28% [15,18]. However, when it comes to the overall lifetime death rates, it is less than 3%, which is fairly low [14,20]. Likewise, 5-year relative survival rate is up to 90.2% in Korean males diagnosed between 2006 and 2010 [17]. Patient stratification based on histology, overall stage, and expected prognosis will be further discussed in the chapter 'E. Treatment'.

C. Screening

Two features of prostate cancer - high incidence and overall good prognosis - put emphasis on the importance of early detection and treatment of this disease. There are two commonly used screening methods – DRE (digital rectal examination) and serum PSA (prostate specific antigen) assay [14].

DRE was used as a primary screening tool for a long time, as it is inexpensive, non-invasive, and easy to perform [21]. However, many researchers have raised questions about its usefulness. Chodak et al. reported that 4160 DREs were performed on 2131 men and 144 prostate biopsies were done, to find out a total of 36 prostate cancers [22]. After the introduction of serum PSA assay in the 1980s, DRE is not regarded as an appropriate screening tool any more in general [14,21].

PSA-based screening started being used widely, and by 2001 around 75% of male populations older than 50 years old had undergone PSA assay [23]. Though it is true that use of serum PSA assay as a screening method helps to detect prostate cancer at an earlier stage, markedly dropping the cancer-related mortality [24], its potential clinical benefit is still questionable [14,25-28]. According to the Prostate cancer Intervention Versus Observation Trial (PIVOT), serum PSA testing and subsequent radical prostatectomy did not improve mortality compared with observation, for 12 years of follow-up period [29]. The European

Randomized Study of Screening for Prostate Cancer (ERSPC) also concluded that more than 1050 men are needed for PSA screening and 37 prostate cancers should be detected in order to prevent single death from prostate cancer [30]. Furthermore, according to the Prostate, Lung, Colorectal, and Ovarian cancer screening trial (PLCO), there was no benefit of reducing mortality from prostate cancer between organized annual PSA screening and opportusnistic PSA screening [31].

Another problem of the serum PSA screening is its false-negativity. According to the National Cancer Institute, there is no lower limit in the PSA value to confirm the absence of cancer cells [14,21]. The Prostate Cancer Prevention Trial also revealed that 15% of males with normal PSA values were actually turned out to have prostate cancer [32]. There have been many trials to develop alternate methods to improve the accuracy of PSA-based screening - such as PSA density, PSA density of transition zone, Prostate cancer gene 3 (PCA3), ultrasensitive PSA, complexed and percent-free PSA, PSA velocity, age-adjusted PSA, frequency of screening, and altering PSA cutoff level. However, none has been found to be superior than total serum PSA assay [14].

Currently, the US Preventive Services Task Force (USPSTF) does not recommend annual PSA screening any more, pointing that there do exist possible harms of PSA-based screening and following radical treatment, such as false-positives, overdiagnosis, and overtreatment [14,33], though that recommendation is still controversial [34,35]. Draisma et al. demonstrated that about 23-42% of men with PSA-detected cancers were actually overdiagnosed [36]. The USPSTF, American College of Physicians (ACP), the American Urological Association (AUA), and the American Cancer Society (ACS) have suggested their own specific screening recommendations, guidance statements, and clinical considerations [37-40].

D. Diagnosis

With increasing use of serum PSA as a screening test, prostate cancer started being suspected at a smaller size, significantly lowering the sensitivity of imaging diagnosis [41]. Multiparametric MRI (magnetic resonance imaging), which uses the combination of conventional anatomical and functional sequences such as diffusion-weighted sequence, dynamic contrast-enhanced sequence, and MR spectroscopy, is known to not only just detect and localize the cancer but also determine its biological behavior such as aggressiveness and invasiveness [42-47]. However, though MRI shows the highest sensitivity in detection and local staging of prostate cancer among all currently available imaging tools, its sensitivity has been reported various from 43% to 96% [41]. Though one recent prospective clinical trial demonstrated that combined MR/PET (positron emission tomography) system has potentially higher sensitivity than PET or MRI alone [48], it needs more cumulated data to prove diagnostic feasibility.

As a result, TRUS(transrectal ultrasonography)-guided systematic random prostate gland biopsy is performed to confirm the diagnosis in most cases, which shows false negative result in 23% of patients at initial biopsy [41]. Particularly, the regions other than the peripheral zone – such as anterior area, apex, and anterolateral horn – are more frequently undersampled by TRUS-guided biopsy, leading to the undergrading or false negativity [49]. Additional biopsies are known to have no significant effect on the detection of cancer [50-52]. Although several US techniques have recently been developed to localize focal prostate cancer more accurately and thus to improve the sensitivity of TRUS-guided biopsy, their contribution is still limited [41].

Recently, many researchers reported that MR-guided target biopsy has higher diagnostic accuracy than TRUS-guided random biopsy, with missed cancer rates as low as 6-10% [53-60]. MR-guided target biopsy is almost always performed in the setting of positive findings of the prostate MR

images, and directly targets the most suspicious region among them. Especially, ventral portions of the prostate gland also can be accurately targeted under the MR guidance, where usually cannot be sampled effectively by TRUS-guided biopsy [61-63]. Correlation between biopsy results and surgical specimen was also more accurate in MR-guided target biopsy than TRUS-guided random biopsy [64-66].

Despite the relatively high diagnostic accuracy, MR-guided biopsy has a significant disadvantage over TRUS-guided biopsy – long procedure time. To achieve optimal imaging quality and accurate needle localization, MR-guided biopsy is usually performed on closed-bore systems, which require significantly longer procedure time (reported median procedure times: 30-68 min) than TRUS-guided biopsy [57,67].

The low sensitivity of imaging diagnosis as well as TRUS or MR-guided biopsy leads to late diagnosis and low cure rate, eventually increasing total medical costs. Therefore it is important to develop a new imaging modality which is capable of diagnosing prostate cancer with higher sensitivity or at least localizing prostate cancer more precisely as more precise localization of prostate cancer might increase biopsy sensitivity.

In general, malignant tissue can be either hypervascular or hypovascular. Prostate cancer is known to have a higher concentration of microvasculature than that of normal prostate tissue [68]. In addition, several angiogenic molecules, such as vascular endothelial growth factor (VEGF), hepatocyte growth factor, and fibroblast growth factor (FGF), have been identified in prostate cancer progression [69-71]. Zhen Jiang et al. demonstrated that NIRS could detect this hemodynamic difference between normal prostate tissue and prostate cancer, consequently imaging prostate cancer with higher sensitivity and specificity than TRUS [72,73]. According to their results, however, TRUS was more accurate in localizing prostate cancer than NIRS, especially in the deep portion of the prostate gland [72,73]. Therefore, it might be possible

to improve the diagnostic accuracy by combining these two modalities [72,73].

E. Treatment

Regarding the treatment strategies of prostate cancer, there is an emerging consensus that low-risk patients do not need any radical treatment - which is now regarded as overtreatment - and conservative management is enough and more appropriate [74]. There are several reasons for coming up to that idea.

First, genetic and molecular hallmarks of cancer are absent in Gleason pattern 3 and present in Gleason pattern 4. Eight generally accepted molecular hallmarks of cancer are as follows: self-sufficiency in growth signal, insensitivity to antigrowth signals, sustained angiogenesis, unlimited replicative potential, local invasion, metastasis, evasion of immune destruction, and de-regulating cellular energetics [75,76]. And there are many genes known to be related to the cancer development, such as AKT, HER2, EGF, EGFR, CKDN1β, DAD1, BCL2, TMPRSS2-ERG, VEGF, CXCR4, etc. All these molecular and genetic hallmarks are absent or minimally expressed in Gleason pattern 3, while they are present or abnormally overexpressed in Gleason pattern 4 [77-89]. It is well known that even Don Gleason himself did not regard Gleason pattern 3 or less as cancer [74].

Second, several autopsy studies revealed that prostate cancer develops in most of elderly men and these cancers are usually smaller than 1cc with low grade histology [90,91]. These results suggest that what affects the cancer mortality is not the presence of cancer cell itself but rather its histologic grade, tumor volume, and patient's age.

Third, many studies consistently demonstrated that Gleason 6 cancer (3+3) rarely metastasizes and thus has no significant impact on the mortality [92-95]. Most of patients who died of low-risk prostate cancer had actually been undergraded at the initial biopsy and turned out to have had higher grade

lesions at the time of diagnosis by later careful review of the specimen [92-95]. Furthermore, a number of previous studies and international associations do not recommend imaging studies, such as CT (computed tomography), MRI, or bone scan, in low-risk patients with prostate cancer for staging, due to the good prognostic nature of the disease [96-100]. Currently, low-risk prostate cancer is defined as Gleason 6 cancer with PSA value less than 10 ng/ml, and those with only one or two positive biopsy cores (regardless of how many cores were sampled) each showing less than 50% cancer involvement and PSA density less than 0.15 are classified as very low-risk cancers [74]. According to the ERSPC, Gleason 6 cancer with volume less than 1.3cc is defined as clinically insignificant cancer [101].

According to the recent review article published in 2014, all Gleason 6 cancers are basically less likely to metastasize and thus do not need any treatment [74]. Nevertheless, authors suggested that Gleason 6 cancers with higher tumor volume still need careful concern, only because of possibility that there is a co-existing occult higher grade cancer, i.e. possibility of undergrading [74]. The concept of active surveillance, neither radical treatment nor watchful waiting, applies to these patients [74]. Active surveillance consists of serial PSA follow-ups and repeating biopsies, and its main goal is to detect patients who need to be reclassified as higher grades. According to one large cohort study, prostate cancer-related mortality was very rare and most men died of other causes such as cardiovascular disease during the period of active surveillance [102]. Another cohort study revealed that the death rate of patients under the policy of watchful waiting tripled after 15 years of follow up [103]. These cohort studies suggest that active surveillance is more appropriate than radical treatment or watchful waiting to the low-risk patients. About 30% of patients with low-risk prostate cancer are known to undergo reclassification into higher grades and become candidate for treatment.

When patients are young with relatively longer life expectancy, the

concept of focal therapy can be applied. Young patients with low-risk prostate cancer and single tumor volume larger than 1.3 cc can be the candidate for the focal therapy [74]. Another candidates for the focal therapy are the patients with clinically insignificant cancer who desire to undergo some interventions for more accurate diagnosis [104]. The 'trifecta' rate – pad and leak free, preserved erectile function, and no evidence of cancer – of the focal therapy is reported up to 84%, which is almost twice higher than that of the conventional radical treatment [105,106]. Prostate cancer mortality under the policy of active surveillance and focal therapy is reported to be 3% at 10 years which is fairly low [102,107].

High-risk - or locally advanced - prostate cancer is known to account for about 15% of all prostate cancers [108]. The definition of this category has been variable over time. D'Amico et al. first defined prostate cancers with clinical T stage ≥ cT2c, a Gleason score ≥ 8, or PSA value over 20 ng/ml as high-risk cancer [109]. The AUA is currently using this definition [110]. The Radiation Therapy Oncology Group (RTOG) defined those with a Gleason score ≥ 8 or a Gleason score ≥ 7 plus either ≥ cT3 or node-positive status as high-risk disease [111]. Recently, the definition of high-risk prostate cancer has been updated more delicately. According to the Cancer of the Prostate Risk Assessment (CAPRA) score, not only PSA value, clinical stage, and Gleason score, but also age and percentage of positive biopsy cores have been included in the definition of this stage [112]. According to the National Comprehensive Cancer Network (NCCN), high-risk prostate cancer is defined as T3a, Gleason score ≥ 8, or PSA value ≥ 20 ng/ml, while very high-risk cancer is defined as T3b or T4 stage, and prognostication is further improved by including the tumor involved proportion of biopsy samples [113].

The first treatment of choice for high-risk prostate cancer is the combination of the radiotherapy and the androgen-deprivation therapy with a curative aim – not only for local disease control but also for completely

eliminating the possibility of metastasis [114]. It is now well-known that the combination of these two modalities is superior to each treatment alone, regardless of the patient's age [115-118]. Especially when the patient is old with shorter life expectancies and considerable comorbidities, this treatment choice is even more suitable than the surgery [119].

The second treatment of choice for high-risk prostate cancer is the radical prostatectomy with the extensive pelvic lymph node dissection [114], sometimes with the post-operative radiotherapy [120,121]. While the surgery is not generally performed to the patients with life expectancies shorter than 10 years [110,122], it is known to be effective in improving the survival rates of the patients with life expectancies longer than 10 years [119,123]. According to the multiple large studies, 10-year prostate cancer-related survival rates were consistently over 90%, which is remarkably favorable [114].

When prostate cancer exceeds the localized status, it sequentially progresses to the following stages: non-castrate rising PSA state, non-castrate metastatic state, and castration-resistant state [114]. The key concept of the treatment strategies for these advanced diseases is a multidisciplinary approach [124,125]. Although the definition of the castration-resistant state is disease progression in the setting of very low levels, so called 'castrate levels', of testosterone, still androgen deprivation therapy is the mainstay of treatment strategies [124]. When the traditional luteinizing hormone releasing hormone (LHRH) analogues with/without LHRH antagonists [126,127] fail to achieve the androgen-deprived status, docetaxel or other several secondary hormonal manipulations - such as steroids, ketoconazole, estrogens, antiandrogens, and antiandrogen withdrawal – can be applied [128,129]. In addition, immunotherapy, androgen biosynthesis inhibition, androgen receptor signaling pathway inhibition, bone-targeted therapy, and chemotherapy have recently been accepted as new effective therapeutic options of castration-resistant prostate cancer [124,125].

4. Purpose of this study

The purpose of this study was to develop a multi-channel NIRS system and verify its diagnostic capability to discriminate focal area mimicking optical properties of prostate cancer from surrounding backgrounds mimicking those of normal prostate gland.

II. Materials and Methods

1. Study #1

A. NIRS signal calculation

We adopted the continuous wave method in our system, and used wavelengths of 785 nm and 830 nm. Modified Beer-Lambert law was used to calculate changes in the concentration of HbO_2 and Hbr [11]. By expanding modified Beer-Lambert law with the given wavelengths of 785 nm and 830 nm, we can get the following equations for changes in the concentration of HbO_2 and Hbr:

$$[\Delta \mathrm{Hb}O_2] = \frac{(\epsilon_{Hbr}^{785nm}\frac{\Delta OD^{830nm}}{B^{830nm}} - \epsilon_{Hbr}^{830nm}\frac{\Delta OD^{785nm}}{B^{785nm}})}{(\epsilon_{Hbr}^{785nm}\epsilon_{HbO_2}^{830nm} - \epsilon_{Hbr}^{830nm}\epsilon_{HbO_2}^{785nm})L}$$

$$[\Delta Hbr] = \frac{(\epsilon_{HbO_2}^{830nm}\frac{\Delta OD^{785nm}}{B^{785nm}} - \epsilon_{HbO_2}^{785nm}\frac{\Delta OD^{830nm}}{B^{830nm}})}{(\epsilon_{Hbr}^{785nm}\epsilon_{HbO_2}^{830nm} - \epsilon_{Hbr}^{830nm}\epsilon_{HbO_2}^{785nm})L}$$

Change in concentration of total hemoglobin (THb) is defined as follows:

$$[\Delta \mathrm{THb}] = [\Delta \mathrm{Hb}O_2] + [\Delta Hbr]$$

B. Development of the multi-channel NIRS system

A total of 16 laser diodes (Thorlabs, USA) – 8 with 785 nm and 8 with 830 nm – were used as the light source in the multi-channel NIRS system. 2 APDs (Avalanche Photo Diode; C5460-01, Hamamatsu, Japan) were used as the detectors.

After passing the band pass filter, light was demodulated into the direct current component by the demodulation circuit using an RMS (Root Mean Square) detector. Signal lost during this demodulation process was compensated by a signal amplifier using OP-Amp. It then underwent low pass filter to remove the remaining modulated component. Finally, it was sampled

by DAQ (Data Acquisition; PCI-6122, National Instruments, Austin, TX, USA), through 2 channels simultaneously.

To determine switching and sampling rates of laser diodes, MCU (microcontroller unit; ATmega128) was used. We set MCU to switch on the laser diodes with 785 nm first, and those with 830 nm second, subsequently. The maximal sampling rate was set at 30 Hz by MCU. Since MCU signal alone was not enough to switch on laser diodes, additional circuit using a transistor was developed. MCU and the computer were connected via RS232c serial communications.

A commercially available power supply with alternate current 220 V was converted into direct current +15 V and -15V. Since most electronic materials used in the system worked with a power supply of 5 V, 12 V, or -12V, Regulator 7805, Regulator 7812, and Regulator 7912 were used, respectively.

Optical fibers with a diameter of 400 μm (FT400-EMT, Thorlabs, USA) were connected to the laser diodes and APDs. To make the emitted light focused, lenses were placed between the laser diodes and optical fibers. The intensity of the emitted laser was set between 5 and 7 mW. Optical fibers linked with the laser diodes and those connected with APDs were respectively placed on the two facing sides of a rectangular material, a temporary substitute for the US probe which was for future use. A diagram and an actual image of the developed NIRS system are shown in figure 1 and 2, respectively.

Computer software named Labview (National Instruments, Austin, TX, USA) was used to develop GUI (Graphic User Interface) which can process the incoming signals and display it on the same monitor simultaneously.

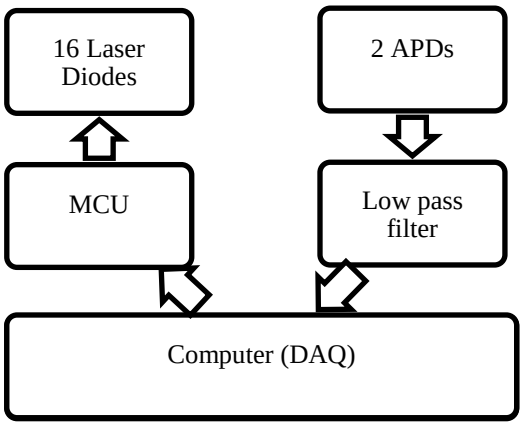

Figure 1. Diagram of the developed multi-channel NIRS system.

Abbreviations: APD = Avalanche Photo Diode, MCU = microcontroller unit, DAQ = data acquisition.

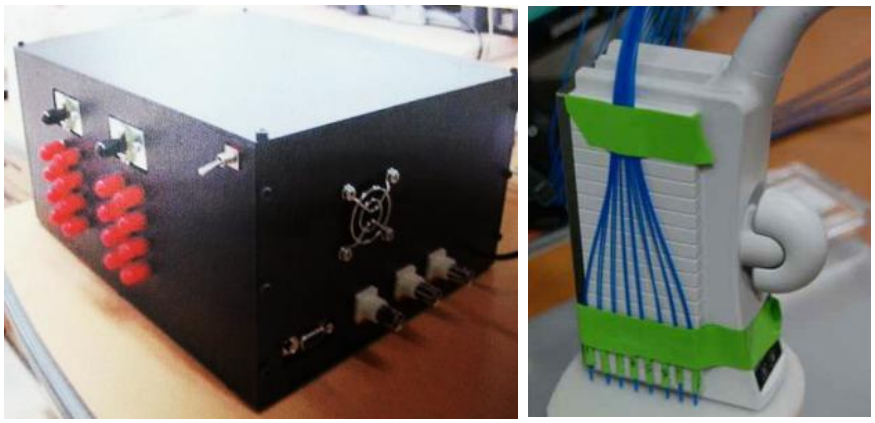

(a) (b)

Figure 2. Actual images of the developed multi-channel NIRS system. (a) External images of the system before connecting optical fibers are shown. 2 optical fibers are linked with 2 detectors in the upper portion and 16 optical fibers are connected with 16 laser diodes in the lower portion. Those on the left side have a wavelength of 785 nm and those on the right side have that of 830 nm. Each optical fiber from one side is paired together with the corresponding one from the other side. (b) 8 sets of the fibers (linked with laser diodes) are placed on one side of the rectangular material, 2 sets of fibers (connected with detectors) are put on the opposite side.

C. Development of the optical phantoms of normal prostate gland and prostate cancer

Two phantom models with optical properties mimicking those of the prostate gland were developed – one with normal prostate gland only and the other with prostate cancer inside. TiO_2 (Titanium dioxide) was used for the scattering effect and India ink was for the absorption effect [104]. Reference values of the optical properties of normal prostate gland, prostate cancer, and surrounding muscle layers were selected from previous studies [130-133], and expressed by adjusting the quantity of TiO_2 and India ink [104]. Fabrication process is as follows:

1) Manually mix TiO_2 with curing agent in a plastic beaker for 5 minutes, and then place it in an ultrasonic bath for 30 minutes. Stir this substance several times during this period.
2) Combine PDMS (Poly-dimethylsiloxane) with India ink by hand mixing in a disposable plastic dish until it becomes completely homogeneous.
3) Interfuse the two suspensions together by hand until they become completely homogeneous. Mixed silicon is made.
4) Place the mixed silicon in a vacuum chamber for approximately 5 minutes (suction power: 30 cmHg).
5) Pour the mixed silicon into a cut and dried mold.
6) Place the mold in a vacuum chamber for approximately 40 minutes with rapid depressurization of the vacuum chamber, to pop a majority of air bubbles (suction power: 30 cmHg for 35 minutes and 40~50 cmHg for the next 5 minutes).
7) Manually puncture the remaining air bubbles with a sharp object for another 40 minutes.
8) The phantom will cure fully in 24 hours at room temperature.

Following the fabrication process, we made a small phantom with optical properties mimicking those of prostate cancer. We then made a couple of larger phantoms with optical properties mimicking those of normal prostate gland. While making one of these normal prostate gland phantoms, we put the prostate cancer phantom into the mixed silicon before pouring the mixed silicon into a mold. Likewise, we then made two even larger phantoms with optical properties similar to those of the muscle layer, putting the two prostate gland phantoms - one of which contains the prostate cancer phantom inside - into these muscle layer phantoms before pouring the mixed silicon into a mold. Diagrams of the two optical phantoms of normal prostate gland and prostate cancer are shown in figure 3. Actual and CT images of these phantoms are shown in figure 4. A detailed specification of the materials used in phantom development is summarized in table 1.

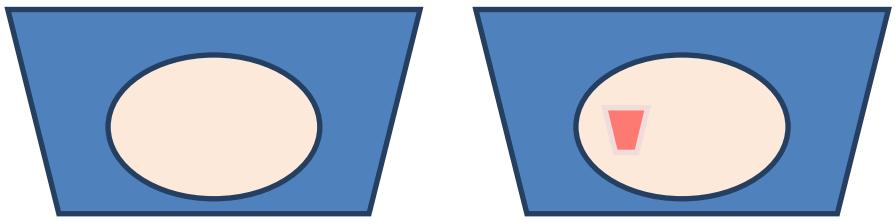

(a) (b)

Figure 3. Diagrams of the developed optical phantoms of (a) normal prostate gland and (b) prostate cancer inside. Blue, white, and pink colors represent the muscle layer, prostate gland, and prostate cancer, respectively.

(a) (b) (c)

Figure 4. (a) Actual and (b, c) CT images of the optical phantoms. On CT images, several microbubbles are seen along the border between the prostate gland and muscle layer portions.

Table 1. Detailed specification of the developed optical phantoms.

	***Size (cm)**	**†Amount (ml)**	**TiO_2 (g)**	**India ink (g)**	**μ_s' (cm^{-1}, 785 nm)**	**μ_a (cm^{-1}, 785 nm)**
Prostate cancer	1.2(w), 1.4(l), 0.8(h)	100	0.084	0.054	7.1	0.41
Prostate gland	4.3(w), 4.5(l), 5.3(h)	200	0.252	0.064	10	0.2
Muscle layer	13(ud), 10(ld), 6(h)	275	0.1	0.045	3.06	0.12

*Final size of a cured phantom. †Amount of mixed silicon prepared.

Abbreviations: μ_s' = induced scattering coefficient, μ_a = absorption coefficient, w = width, l = length, h = height, ud = diameter of upper face, ld = diameter of lower face.

D. Verification of the multi-channel NIRS system with the optical phantom model of prostate cancer

We applied our multi-channel NIRS system to the optical phantom models of prostate gland and prostate cancer to verify its diagnostic capability. We placed a rectangular material, containing 8 sets of laser diodes and 2 detectors on its two facing sides, respectively, over the phantoms we developed. The expected routes of light passage from the laser diodes to the detectors are shown in figure 5. We measured the light intensity passing through the both phantoms at each channel and calculated the differences by subtracting one from another.

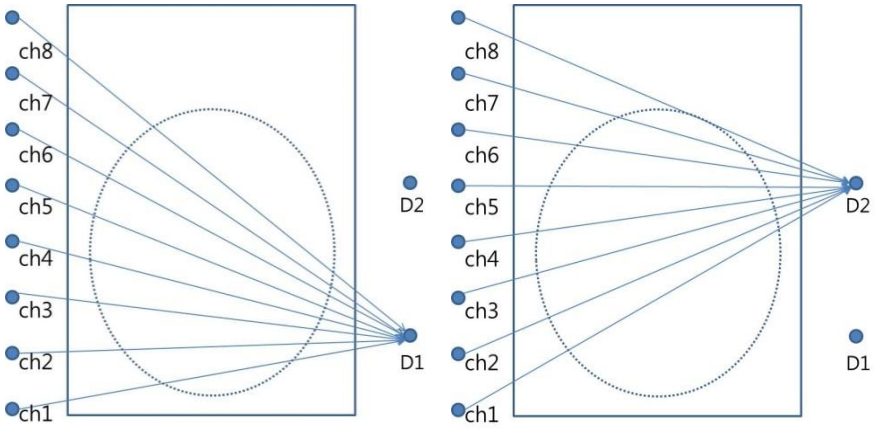

(a) (b)

Figure 5. Expected routes of light passage from 8 sets of laser diodes to 2 detectors. Dotted oval circle represents the phantom mimicking optical properties of the prostate gland.

Abbreviations: ch = channel of laser diodes, D = detector.

2. Study #2

A. Upgrade of the NIRS system

After the first verification study, we added 2 more APDs (to have a total of 4 APDs) to improve the spatial resolution and the field of view. We also developed the plastic holder containing 12 holes with the same diameter as the optical fibers. These holes were designed in order to hold the optical fibers firmly, preventing them from the motion during the signal acquisition which was thought to be the major cause of signal noise and low reproducibility. The arrangement of the sources and detectors were also changed to be located symmetrically on the both sides of the plastic holder, in order to minimize the interferences caused by nearby sources (figure 6a, b).

We adopted open source platform named Nirfast (Dartmouth College and University of Birmingham, Birmingham, United Kingdom) for modeling NIR light transport inside the phantom [134,135]. This software, coded on the basis of MATLAB (MathWorks, USA), is capable of retrieving the absorption coefficient from the single wavelength light attenuation and reconstructing it into 2D images. As Nirfast can work on the single wavelength light, we decided to use only 785 nm fibers in order to optimize the signal acquisition. Labview software was also upgraded to be compatible with the new setting of 4 detectors and single wavelength of 785 nm.

B. Verification of the upgraded NIRS system with the black-colored eraser embedded inside the normal prostate optical phantom

We developed another optical phantom of normal prostate gland following the same fabrication process mentioned above, except for the following three things: 1) We used the vacuum oven rather than the vacuum chamber in order to keep high temperature during the curing process. 2) The vacuum pump was upgraded to the more powerful one. 3) The black-colored

eraser rather than the optical prostate cancer phantom was embedded inside (figure 6c). The reasons for these changes were to minimize the internal air bubbles and to maximize the difference of optical properties. We placed the plastic holder containing a total of 12 optical fibers (8 sources and 4 detectors) over the developed phantom, and measured NIRS signal attenuation, which was used to reconstruct the 2D images by Nirfast algorithm (figure 6d). We repeated signal measurements four times, changing the locations of the plastic holder over the black-colored eraser.

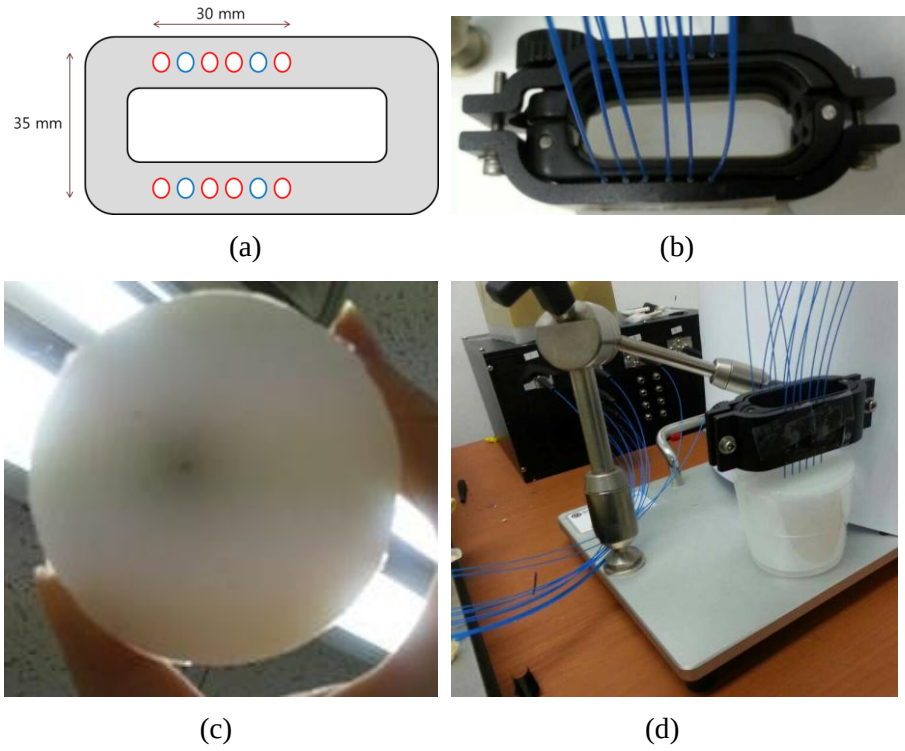

Figure 6. Upgraded NIRS system and the optical phantom of the prostate gland with the black-colored eraser embedded inside. (a) Diagram of the plastic holder containing 12 holes is shown. Red holes are to contain source fibers with wavelength of 785 nm, while blue ones are for detector fibers. (b) Actual image of the plastic holder with its 12 holes each containing optical fibers is seen. (c) The black-colored eraser is embedded inside the optical phantom of normal prostate gland. (d) The plastic holder and optical fibers are placed over the developed phantom.

3. Study #3 – Materials and Methods

A. Rearrangement of the optical fibers to suit the TRUS probe guide

We rearranged the optical fibers to suit the TRUS probe guide (EC9-4, Siemens Medical Solutions, CA, USA), as we wanted to validate the possibility of fusion device between TRUS and NIRS. While basic arrangement was same as the previous plastic holder - 4 sources and 2 detectors on each side, the distance between the fibers was reduced to fit the narrow guide, and the fibers were bonded each other by Epoxy to be fixed in position. We also made four grooves on each side of the guide tightly fitting the fixed set of the optical fibers (figure 7).

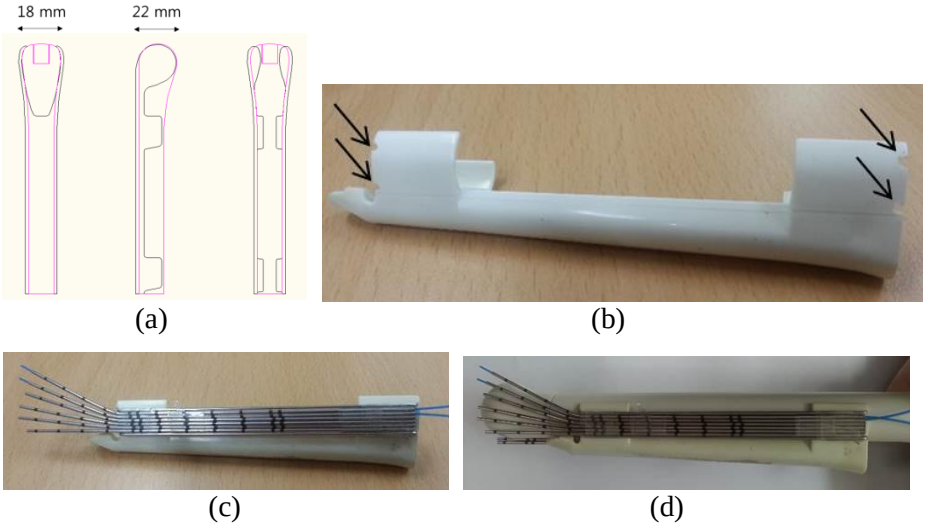

Figure 7. Rearrangement of the optical fibers to suit the TRUS probe guide. (a) Diagrams of the TRUS guide probe are seen. (b) Four grooves (arrows) are made on each side of the TRUS guide probe (8 grooves in total), designed to hold the optical fibers tightly preventing them from the motion. (c) 6 optical fibers are bonded each other by Epoxy and placed on one side of the TRUS guide probe. (d) The TRUS probe, the guide, and the optical fibers are all held together.

B. Development of the new optical phantom of prostate cancer with semicircular surface contour

We developed the new optical phantom of prostate cancer with semicircular surface contour, following the basically same fabrication process as before. First, we developed the phantom mimicking optical properties of muscle layer, top side of which were shaped semicircular. We then fabricated the small phantom of prostate cancer, and put it over the semicircular surface of the muscle layer phantom. Finally, we made the phantom of normal prostate gland over the semicircular surface of the muscle layer phantom, surrounding the prostate cancer phantom (figure 8a, b).

C. Verification of the rearranged optical fibers with the new phantom

We virtually divided the developed optical phantom into 5 regions (from *A* to *E*), and measured NIRS signal attenuation at each region. The optical prostate cancer phantom was located mainly at the region *D*, slightly extending to the margin of region *E* (figure 8c). Measured light signal attenuations were converted into the absorption coefficients to reconstruct the 2D image mapping.

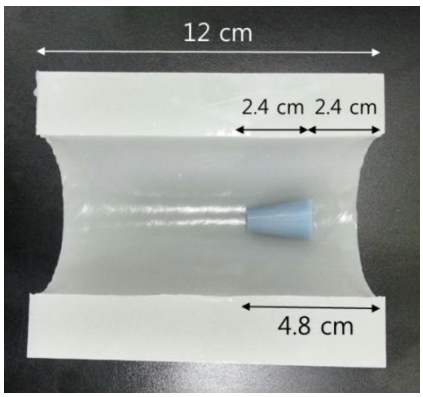

(a)

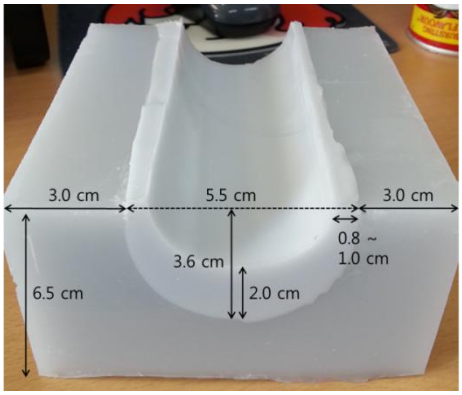

(b)

(c)

Figure 8. Development of the new optical phantom of the prostate cancer with semicircular surface contour. (a) The small optical prostate cancer phantom is placed over the semicircular-shaped top side of the optical muscle layer phantom. (b) The optical phantom of normal prostate gland is added over the optical phantom of muscle layer, surrounding the optical prostate cancer phantom inside. (c) NIRS optical fibers fixed on the TRUS probe guide are placed over the developed optical phantom. The fibers are taped each other to be fixed more tightly in position.

III. Results

1. Study #1

Light signal intensities of the prostate cancer phantom subtracted from that of the normal prostate gland phantom is shown in figure 9. Relatively lower values were seen around channel 3, 4, and 5 at both detectors and at both wavelengths, suggesting that light is more absorbed and/or scattered when passing through these routes, reflecting the presence of an inner region with different optical properties from its surroundings.

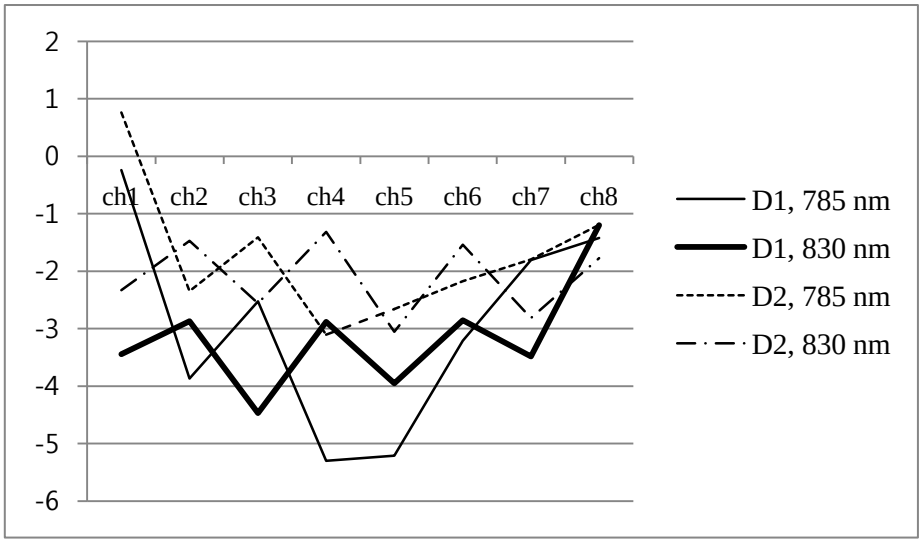

Figure 9. Light signal intensities of the prostate cancer phantom subtracted from that of the normal prostate gland phantom. Relatively lower values are seen around channel 3, 4, and 5 at the both detectors.

Abbreviations: ch = channel of laser diodes, D = detector.

2. Study #2

On figure 10, location of the plastic holder, reconstructed 2D images based on absorption coefficients, and overlaid images of the both are shown. As we changed the location of the optical fibers, area of high absorption coefficients were also changed, suggesting the capability of the upgraded NIRS system to reliably distinguish inner regions with different optical properties.

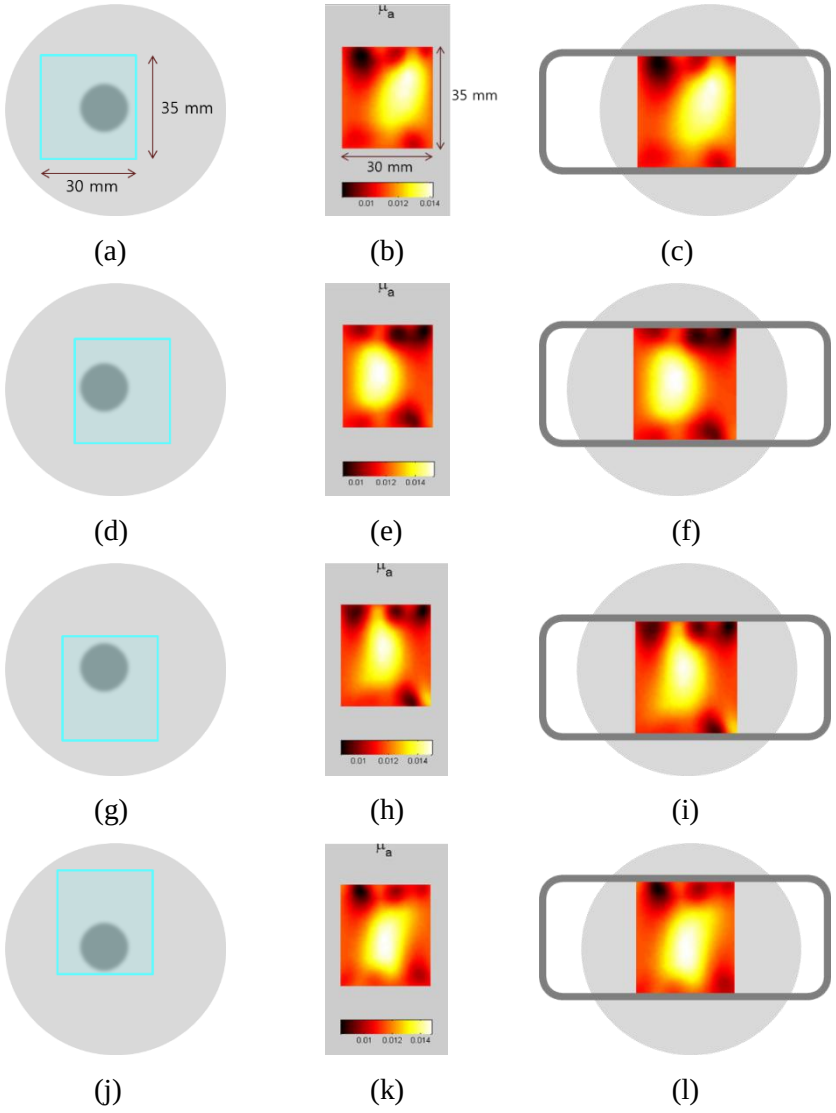

Figure 10. Reconstructed 2D images, obtained by the upgraded NIRS system using the optical prostate phantom with the black-colored eraser inside. (a, d, g, j) The first row shows the four different locations of the NIRS optical fibers (blue box) placed over the embedded black-colored eraser (central black circle). (b, e, h, k) The second row shows the reconstructed 2D images based on absorption coefficients. (c, f, i, l) Overlaid images of the phantom and the reconstructed 2D images are shown at the third row. Areas of high absorption coefficients are correlated with the location of the black-colored eraser.

3. Study #3

Measured absorption coefficients were higher at the region *D* and *E* than the other three regions (figure 11). The absorption coefficients of the region *C* were higher than the region *A* and *B* and lower than the region *D* and *E*. Considering the location of the optical prostate cancer phantom, these results suggest the capability of the rearranged NIRS fibers fixed with the TRUS probe guide to locate the focal region with different optical properties from surroundings.

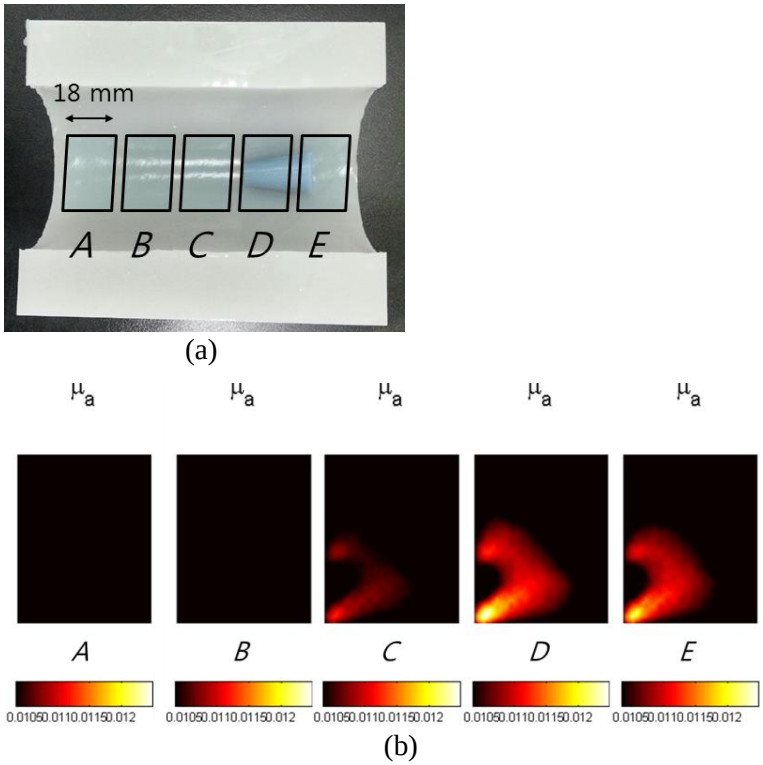

Figure 11. Reconstructed 2D images of the absorption coefficients measured upon the optical prostate cancer phantom with semicircular surface contour. (a) We virtually divided the optical phantom into 5 regions (from *A* to *E*) and measured NIRS signal attenuation at each region. (b) Reconstructed 2D images based on the absorption coefficients are seen. Region *D* and *E* show higher absorption coefficients than the other three regions, correlating with the location of the embedded optical phantom of prostate cancer.

IV. Discussion

Prostate cancer lesions are known to have increased density of capillaries compared to the surrounding benign prostate tissue [68]. Zhen Jiang et al. demonstrated that NIRS could differentiate prostate cancer from the surrounding normal prostate gland using differences in optical properties caused by different degrees of vascularity, with better sensitivity and specificity than TRUS [72,73].

We anticipated that NIRS data would provide additional information about the localization of focal prostate cancer. This phantom study was an initial step for the development of a new NIRS imaging system and verifying its diagnostic capability with the optical phantoms of prostate cancer.

On study #1, NIR lights were relatively more attenuated around the channel 3, 4, and 5 than the other channels, reflecting the presence of an inner region with different optical properties from its surroundings along the light-travelling routes of these channels. Though this result was somewhat encouraging, there exist two major limitations in this result. First, as our first phantom was developed without precise information about the location of its internal components, whether the prostate cancer component was actually located around the channel 3, 4, and 5 is still questionable. Second, discrimination of these three channels from the others was not as prominent as expected. There can be several possible explanations for this little difference of the NIR light attenuation degrees. First, CT scan revealed that there were several small air bubbles around the border between the normal prostate gland and muscle layer portions, which could have been the source of signal noise. Second, the NIRS optical fibers were not firmly fixed in position, possibly lowering the reproducibility and reliability of the measurement. Third, interference effects of the NIR lights on the nearby channels could have existed, also possibly causing the signal noise.

On study #2, we upgraded our NIRS system and the fabrication process of the optical phantom development to optimize the system and to minimize the limitations of study #1. We adopted Nirfast algorithm to reconstruct 2D images, which became possible by adding 2 more detectors to improve the spatial resolution and field of view. As we developed the plastic holder to set each optical fiber in the same position during the measurement, the received signals were remarkably more consistent repeatedly than study #1. In addition, delineation of the focal area with high absorption coefficients from the surroundings was more prominent than study #1, and well correlated with the actual location of the target region. There can be three possible reasons for this. First, we changed arrangement of the optical fibers. On study #1, the sources and the detectors were separated on each side, making light travel uni-directionally. In this case, interference effects of nearby channels cannot be compensated, resulting in the measurement error. On study #2, the sources and the detectors were placed symmetrically on the both sides, letting light pass bi-directionally. Though interference effects do exist even in this setting, they affect each combination of the source-detector to the same degree and therefore can be ignored when it comes to evaluating relative differences. Second, we used the vacuum oven and the more powerful vacuum pump to minimize the air bubbles, the possible source of signal noise. Third, we used the black-colored eraser rather than the optical prostate cancer phantom, maximizing the optical differences between the target region and its surroundings.

As we wanted to validate diagnostic capability of the NIRS system when it is combined with TRUS, we rearranged the optical fibers to suit the TRUS probe guide and developed the new optical phantom of prostate cancer with semicircular contour on study #3. The reason that we made top of the phantom semicircular-shaped was to mimic the actual contour between the TRUS probe and the rectal wall during the TRUS examination. Area with

high absorption coefficients were well correlated with the actual location of the optical prostate cancer phantom, successfully demonstrating diagnostic capability of the NIRS system with the geometry suitable for the TRUS probe guide to distinguish the optical prostate cancer phantom from the surrounding optical normal prostate gland phantom.

Further studies are inevitable to develop a clinically feasible NIRS system. First, an *ex vivo* study with surgical specimen of the human prostate cancer needs to be done. Second, an animal study using the prostate cancer model should be performed to verify *in vivo* diagnostic performance of this new imaging modality. Unlike the artificially developed optical phantoms, as not only NIRS but also TRUS can be performed on these two *ex vivo* and *in vivo* models, an algorithm for image registration between NIRS and TRUS can be set up and optimized. Third, a clinical study with prostate cancer patients should be taken to validate and optimize its diagnostic performance on human bodies. Fourth, whether NIRS can actually provide additional information about the localization of focal prostate cancer and thus can be used as a guide for selecting target biopsy sites should be verified. Finally, contribution of this new imaging modality to the overall diagnostic accuracy of prostate cancer should be assessed.

V. Conclusion

We successfully demonstrated possibility of our NIRS system as a new potential imaging method for improvement of diagnostic accuracy in localization of focal prostate cancer. In future, the NIRS system will possibly be combined with TRUS, improving diagnostic accuracy of prostate cancer imaging and localization of target biopsy sites.

References

1. Siesler HW, Ozaki Y, Kawata S, Heise HM. Near-infrared spectroscopy: principles, instruments, applications: John Wiley & Sons; 2008.
2. Ferrari M, Quaresima V. A brief review on the history of human functional near-infrared spectroscopy (fNIRS) development and fields of application. Neuroimage 2012;63:921-35.
3. Chance B. Optical method. Annu Rev Biophys Biophys Chem 1991;20:1-28.
4. Jobsis FF. Noninvasive, infrared monitoring of cerebral and myocardial oxygen sufficiency and circulatory parameters. Science 1977;198:1264-7.
5. Piantadosi CA. Early development of near-infrared spectroscopy at Duke University. J Biomed Opt 2007;12:062102.
6. Delpy D, Cope M. Quantification in tissue near–infrared spectroscopy. Philosophical Transactions of the Royal Society of London. Series B: Biological Sciences 1997;352:649-59.
7. Yodh A, Chance B. Spectroscopy and imaging with diffusing light. Physics Today 1995;48:34.
8. Rolfe P. In vivo near-infrared spectroscopy. Annual review of biomedical engineering 2000;2:715-54.
9. Scholkmann F, Kleiser S, Metz AJ, Zimmermann R, Mata Pavia J, Wolf U, et al. A review on continuous wave functional near-infrared spectroscopy and imaging instrumentation and methodology. Neuroimage 2014;85 Pt 1:6-27.
10. Torricelli A, Contini D, Pifferi A, Caffini M, Re R, Zucchelli L, et al. Time domain functional NIRS imaging for human brain mapping. Neuroimage 2014;85 Pt 1:28-50.
11. Delpy DT, Cope M, Van der Zee P, Arridge S, Wray S, Wyatt J. Estimation of optical pathlength through tissue from direct time of flight measurement. Physics in medicine and biology 1988;33:1433.
12. Beer A. Bestimmung der Absorption des rothen Lichts in farbigen Flüssigkeiten. Annalen der Physik 1852;162:78-88.
13. Lambert JH. Lamberts Photometrie:(Photometria, sive De mensura et gradibus luminis, colorum et umbrae)(1760): W. Engelmann; 1892.
14. Ragsdale JW, 3rd, Halstater B, Martinez-Bianchi V. Prostate Cancer Screening. Prim Care 2014;41:355-70.
15. American Cancer Society. Prostate Cancer. 2013. Available at: http://www.cancer.org/cancer/prostatecancer/detailedguide/prostate-cancer-key-statistics. Accessed January 4, 2014.
16. Siegel R, Naishadham D, Jemal A. Cancer statistics, 2013. CA Cancer J Clin 2013;63:11-30.

17. Jung KW, Won YJ, Kong HJ, Oh CM, Seo HG, Lee JS. Cancer statistics in Korea: incidence, mortality, survival and prevalence in 2010. Cancer Res Treat 2013;45:1-14.
18. Saman DM, Lemieux AM, Nawal Lutfiyya M, Lipsky MS. A review of the current epidemiology and treatment options for prostate cancer. Dis Mon 2014;60:150-4.
19. Giovannucci E, Liu Y, Platz EA, Stampfer MJ, Willett WC. Risk factors for prostate cancer incidence and progression in the health professionals follow-up study. Int J Cancer 2007;121:1571-8.
20. American Cancer Society. Lifetime risk of developing or dying from cancer. 2013. Available at: http://www.cancer.org/cancer/cancerbasics/lifetime-probability-of-developing-or-dying-from-cancer. Accessed January 4, 2014.
21. National Cancer Institute at the National Institutes of Health. Prostate cancer screening (PDQ). Available at: http://www.cancer.gov/cancertopics/pdq/screening/prostate/HealthProfessional/page3#Reference3.10. Accessed January 5, 2014.
22. Chodak GW, Keller P, Schoenberg HW. Assessment of screening for prostate cancer using the digital rectal examination. J Urol 1989;141:1136-8.
23. Sirovich BE, Schwartz LM, Woloshin S. Screening men for prostate and colorectal cancer in the United States: does practice reflect the evidence? JAMA 2003;289:1414-20.
24. Jemal A, Siegel R, Xu J, Ward E. Cancer statistics, 2010. CA Cancer J Clin 2010;60:277-300.
25. Heidenreich A, Bastian PJ, Bellmunt J, Bolla M, Joniau S, van der Kwast T, et al. EAU guidelines on prostate cancer. part 1: screening, diagnosis, and local treatment with curative intent-update 2013. Eur Urol 2014;65:124-37.
26. Djulbegovic M, Beyth RJ, Neuberger MM, Stoffs TL, Vieweg J, Djulbegovic B, et al. Screening for prostate cancer: systematic review and meta-analysis of randomised controlled trials. BMJ 2010;341:c4543.
27. Chou R, Croswell JM, Dana T, Bougatsos C, Blazina I, Fu R, et al. Screening for prostate cancer: a review of the evidence for the U.S. Preventive Services Task Force. Ann Intern Med 2011;155:762-71.
28. American Urologic Association. Early detection of prostate cancer: AUA guideline. 2013. Available at: http://www.auanet.org/common/pdf/education/clinical-guidance/Prostate-Cancer-Detection.pdf. Accessed January 5, 2014.
29. Wilt TJ, Brawer MK, Barry MJ, Jones KM, Kwon Y, Gingrich JR, et al. The Prostate cancer Intervention Versus Observation Trial:VA/NCI/AHRQ Cooperative Studies Program #407 (PIVOT):

design and baseline results of a randomized controlled trial comparing radical prostatectomy to watchful waiting for men with clinically localized prostate cancer. Contemp Clin Trials 2009;30:81-7.
30. Schroder FH, Hugosson J, Roobol MJ, Tammela TL, Ciatto S, Nelen V, et al. Screening and prostate-cancer mortality in a randomized European study. N Engl J Med 2009;360:1320-8.
31. Pinsky PF, Parnes HL, Andriole G. Mortality and complications after prostate biopsy in the Prostate, Lung, Colorectal and Ovarian Cancer Screening (PLCO) trial. BJU Int 2014;113:254-9.
32. Thompson IM, Pauler DK, Goodman PJ, Tangen CM, Lucia MS, Parnes HL, et al. Prevalence of prostate cancer among men with a prostate-specific antigen level < or =4.0 ng per milliliter. N Engl J Med 2004;350:2239-46.
33. US Preventive Services Task Force. Screening for Prostate Cancer. 2012. Available at: http://www.uspreventiveservicestaskforce.org/prostatecancerscreening.htm. Accessed January 8, 2014.
34. Glass AS, Cowan JE, Fuldeore MJ, Cooperberg MR, Carroll PR, Kenfield SA, et al. Patient demographics, quality of life, and disease features of men with newly diagnosed prostate cancer: trends in the PSA era. Urology 2013;82:60-5.
35. Ilic D, Neuberger MM, Djulbegovic M, Dahm P. Screening for prostate cancer. Cochrane Database Syst Rev 2013;1:CD004720.
36. Draisma G, Etzioni R, Tsodikov A, Mariotto A, Wever E, Gulati R, et al. Lead time and overdiagnosis in prostate-specific antigen screening: importance of methods and context. J Natl Cancer Inst 2009;101:374-83.
37. American College of Physicians. ACP guidance statements: Screening for Prostate Cancer. Available at: http://annals.org/article.aspx?articleID51676183&atab57. .
38. American Urological Association. AUA Guideline on Early Detection of Prostate Cancer. Available at: http://www.auanet.org/education/guidelines/prostate-cancer-detection.cfm.
39. American Cancer Society. ACS Guideline for the Early Detection of Prostate Cancer. Available at: http://mr.crossref.org/iPage?doi510.3322%2Fcaac.20066.
40. US Preventive Services Task Force. Talking with your patients about screening for prostate cancer. 2012. Available at: http://www.uspreventiveservicestaskforce.org/prostatecancerscreening/prostatecancerscript.pdf. Accessed January 5, 2014.
41. Talab SS, Preston MA, Elmi A, Tabatabaei S. Prostate cancer imaging: what the urologist wants to know. Radiol Clin North Am

2012;50:1015-41.
42. Mullerad M, Hricak H, Kuroiwa K, Pucar D, Chen HN, Kattan MW, et al. Comparison of endorectal magnetic resonance imaging, guided prostate biopsy and digital rectal examination in the preoperative anatomical localization of prostate cancer. J Urol 2005;174:2158-63.
43. Johnson LM, Turkbey B, Figg WD, Choyke PL. Multiparametric MRI in prostate cancer management. Nat Rev Clin Oncol 2014.
44. Tanimoto A, Nakashima J, Kohno H, Shinmoto H, Kuribayashi S. Prostate cancer screening: the clinical value of diffusion-weighted imaging and dynamic MR imaging in combination with T2-weighted imaging. J Magn Reson Imaging 2007;25:146-52.
45. Delongchamps NB, Beuvon F, Eiss D, Flam T, Muradyan N, Zerbib M, et al. Multiparametric MRI is helpful to predict tumor focality, stage, and size in patients diagnosed with unilateral low-risk prostate cancer. Prostate Cancer Prostatic Dis 2011;14:232-7.
46. Delongchamps NB, Rouanne M, Flam T, Beuvon F, Liberatore M, Zerbib M, et al. Multiparametric magnetic resonance imaging for the detection and localization of prostate cancer: combination of T2-weighted, dynamic contrast-enhanced and diffusion-weighted imaging. BJU Int 2011;107:1411-8.
47. Fennessy FM, McKay RR, Beard CJ, Taplin ME, Tempany CM. Dynamic contrast-enhanced magnetic resonance imaging in prostate cancer clinical trials: potential roles and possible pitfalls. Transl Oncol 2014;7:120-9.
48. Hartenbach M, Hartenbach S, Bechtloff W, Danz B, Kraft K, Klemenz B, et al. Combined PET/MRI Improves Diagnostic Accuracy in Patients with Prostate Cancer: A Prospective Diagnostic Trial. Clin Cancer Res 2014.
49. Patel MI, DeConcini DT, Lopez-Corona E, Ohori M, Wheeler T, Scardino PT. An analysis of men with clinically localized prostate cancer who deferred definitive therapy. J Urol 2004;171:1520-4.
50. Roehl KA, Antenor JA, Catalona WJ. Serial biopsy results in prostate cancer screening study. J Urol 2002;167:2435-9.
51. Djavan B, Milani S, Remzi M. Prostate biopsy: who, how and when. An update. Can J Urol 2005;12 Suppl 1:44-8; discussion 99-100.
52. Lujan M, Paez A, Santonja C, Pascual T, Fernandez I, Berenguer A. Prostate cancer detection and tumor characteristics in men with multiple biopsy sessions. Prostate Cancer Prostatic Dis 2004;7:238-42.
53. D'Amico AV, Tempany CM, Cormack R, Hata N, Jinzaki M, Tuncali K, et al. Transperineal magnetic resonance image guided prostate biopsy. J Urol 2000;164:385-7.
54. Cormack RA, D'Amico AV, Hata N, Silverman S, Weinstein M, Tempany CM. Feasibility of transperineal prostate biopsy under

interventional magnetic resonance guidance. Urology 2000;56:663-4.
55. Beyersdorff D, Winkel A, Hamm B, Lenk S, Loening SA, Taupitz M. MR imaging-guided prostate biopsy with a closed MR unit at 1.5 T: initial results. Radiology 2005;234:576-81.
56. Pondman KM, Futterer JJ, ten Haken B, Schultze Kool LJ, Witjes JA, Hambrock T, et al. MR-guided biopsy of the prostate: an overview of techniques and a systematic review. Eur Urol 2008;54:517-27.
57. Overduin CG, Futterer JJ, Barentsz JO. MRI-guided biopsy for prostate cancer detection: a systematic review of current clinical results. Curr Urol Rep 2013;14:209-13.
58. Zangos S, Eichler K, Engelmann K, Ahmed M, Dettmer S, Herzog C, et al. MR-guided transgluteal biopsies with an open low-field system in patients with clinically suspected prostate cancer: technique and preliminary results. Eur Radiol 2005;15:174-82.
59. Engehausen DG, Engelhard K, Schwab SA, Uder M, Wach S, Wullich B, et al. Magnetic resonance image-guided biopsies with a high detection rate of prostate cancer. ScientificWorldJournal 2012;2012:975971.
60. Hoeks CM, Schouten MG, Bomers JG, Hoogendoorn SP, Hulsbergen-van de Kaa CA, Hambrock T, et al. Three-Tesla magnetic resonance-guided prostate biopsy in men with increased prostate-specific antigen and repeated, negative, random, systematic, transrectal ultrasound biopsies: detection of clinically significant prostate cancers. Eur Urol 2012;62:902-9.
61. Sakai I, Harada K, Hara I, Eto H, Miyake H. A comparison of the biological features between prostate cancers arising in the transition and peripheral zones. BJU Int 2005;96:528-32.
62. Cheng L, Jones TD, Pan CX, Barbarin A, Eble JN, Koch MO. Anatomic distribution and pathologic characterization of small-volume prostate cancer (<0.5 ml) in whole-mount prostatectomy specimens. Mod Pathol 2005;18:1022-6.
63. Lawrentschuk N, Haider MA, Daljeet N, Evans A, Toi A, Finelli A, et al. 'Prostatic evasive anterior tumours': the role of magnetic resonance imaging. BJU Int 2010;105:1231-6.
64. Hambrock T, Hoeks C, Hulsbergen-van de Kaa C, Scheenen T, Futterer J, Bouwense S, et al. Prospective assessment of prostate cancer aggressiveness using 3-T diffusion-weighted magnetic resonance imaging-guided biopsies versus a systematic 10-core transrectal ultrasound prostate biopsy cohort. Eur Urol 2012;61:177-84.
65. Steinberg DM, Sauvageot J, Piantadosi S, Epstein JI. Correlation of prostate needle biopsy and radical prostatectomy Gleason grade in academic and community settings. Am J Surg Pathol 1997;21:566-76.

66. Coogan CL, Latchamsetty KC, Greenfield J, Corman JM, Lynch B, Porter CR. Increasing the number of biopsy cores improves the concordance of biopsy Gleason score to prostatectomy Gleason score. BJU Int 2005;96:324-7.
67. Irani J, Fournier F, Bon D, Gremmo E, Dore B, Aubert J. Patient tolerance of transrectal ultrasound-guided biopsy of the prostate. Br J Urol 1997;79:608-10.
68. Bigler SA, Deering RE, Brawer MK. Comparison of microscopic vascularity in benign and malignant prostate tissue. Hum Pathol 1993;24:220-6.
69. Doll JA, Reiher FK, Crawford SE, Pins MR, Campbell SC, Bouck NP. Thrombospondin-1, vascular endothelial growth factor and fibroblast growth factor-2 are key functional regulators of angiogenesis in the prostate. Prostate 2001;49:293-305.
70. Huss WJ, Barrios RJ, Foster BA, Greenberg NM. Differential expression of specific FGF ligand and receptor isoforms during angiogenesis associated with prostate cancer progression. Prostate 2003;54:8-16.
71. Morrissey C, Dowell A, Koreckij TD, Nguyen H, Lakely B, Fanslow WC, et al. Inhibition of angiopoietin-2 in LuCaP 23.1 prostate cancer tumors decreases tumor growth and viability. Prostate 2010;70:1799-808.
72. Jiang Z, Holyoak GR, Bartels KE, Ritchey JW, Xu G, Bunting CF, et al. In vivo trans-rectal ultrasound-coupled optical tomography of a transmissible venereal tumor model in the canine pelvic canal. J Biomed Opt 2009;14:030506.
73. Jiang Z, Piao D, Holyoak GR, Ritchey JW, Bartels KE, Slobodov G, et al. Trans-rectal ultrasound-coupled spectral optical tomography of total hemoglobin concentration enhances assessment of the laterality and progression of a transmissible venereal tumor in canine prostate. Urology 2011;77:237-42.
74. Klotz L, Emberton M. Management of low risk prostate cancer-active surveillance and focal therapy. Nat Rev Clin Oncol 2014.
75. Hanahan D, Weinberg RA. The hallmarks of cancer. Cell 2000;100:57-70.
76. Hanahan D, Weinberg RA. Hallmarks of cancer: the next generation. Cell 2011;144:646-74.
77. Skacel M, Ormsby AH, Pettay JD, Tsiftsakis EK, Liou LS, Klein EA, et al. Aneusomy of chromosomes 7, 8, and 17 and amplification of HER-2/neu and epidermal growth factor receptor in Gleason score 7 prostate carcinoma: a differential fluorescent in situ hybridization study of Gleason pattern 3 and 4 using tissue microarray. Hum Pathol 2001;32:1392-7.

78. Susaki E, Nakayama KI. Multiple mechanisms for p27(Kip1) translocation and degradation. Cell Cycle 2007;6:3015-20.
79. Padar A, Sathyanarayana UG, Suzuki M, Maruyama R, Hsieh JT, Frenkel EP, et al. Inactivation of cyclin D2 gene in prostate cancers by aberrant promoter methylation. Clin Cancer Res 2003;9:4730-4.
80. Guo Y, Sklar GN, Borkowski A, Kyprianou N. Loss of the cyclin-dependent kinase inhibitor p27(Kip1) protein in human prostate cancer correlates with tumor grade. Clin Cancer Res 1997;3:2269-74.
81. True L, Coleman I, Hawley S, Huang CY, Gifford D, Coleman R, et al. A molecular correlate to the Gleason grading system for prostate adenocarcinoma. Proc Natl Acad Sci U S A 2006;103:10991-6.
82. Fleischmann A, Huland H, Mirlacher M, Wilczak W, Simon R, Erbersdobler A, et al. Prognostic relevance of Bcl-2 overexpression in surgically treated prostate cancer is not caused by increased copy number or translocation of the gene. Prostate 2012;72:991-7.
83. Tomlins SA, Mehra R, Rhodes DR, Cao X, Wang L, Dhanasekaran SM, et al. Integrative molecular concept modeling of prostate cancer progression. Nat Genet 2007;39:41-51.
84. Hendriksen PJ, Dits NF, Kokame K, Veldhoven A, van Weerden WM, Bangma CH, et al. Evolution of the androgen receptor pathway during progression of prostate cancer. Cancer Res 2006;66:5012-20.
85. Bismar TA, Dolph M, Teng LH, Liu S, Donnelly B. ERG protein expression reflects hormonal treatment response and is associated with Gleason score and prostate cancer specific mortality. Eur J Cancer 2012;48:538-46.
86. Furusato B, Gao CL, Ravindranath L, Chen Y, Cullen J, McLeod DG, et al. Mapping of TMPRSS2-ERG fusions in the context of multi-focal prostate cancer. Mod Pathol 2008;21:67-75.
87. Wang J, Cai Y, Ren C, Ittmann M. Expression of variant TMPRSS2/ERG fusion messenger RNAs is associated with aggressive prostate cancer. Cancer Res 2006;66:8347-51.
88. West AF, O'Donnell M, Charlton RG, Neal DE, Leung HY. Correlation of vascular endothelial growth factor expression with fibroblast growth factor-8 expression and clinico-pathologic parameters in human prostate cancer. Br J Cancer 2001;85:576-83.
89. Erbersdobler A, Isbarn H, Dix K, Steiner I, Schlomm T, Mirlacher M, et al. Prognostic value of microvessel density in prostate cancer: a tissue microarray study. World J Urol 2010;28:687-92.
90. Sakr WA, Grignon DJ, Crissman JD, Heilbrun LK, Cassin BJ, Pontes JJ, et al. High grade prostatic intraepithelial neoplasia (HGPIN) and prostatic adenocarcinoma between the ages of 20-69: an autopsy study of 249 cases. In Vivo 1994;8:439-43.
91. Zlotta AR, Egawa S, Pushkar D, Govorov A, Kimura T, Kido M, et al.

Prevalence of prostate cancer on autopsy: cross-sectional study on unscreened Caucasian and Asian men. J Natl Cancer Inst 2013;105:1050-8.
92. Porten SP, Whitson JM, Cowan JE, Cooperberg MR, Shinohara K, Perez N, et al. Changes in prostate cancer grade on serial biopsy in men undergoing active surveillance. J Clin Oncol 2011;29:2795-800.
93. Ross HM, Kryvenko ON, Cowan JE, Simko JP, Wheeler TM, Epstein JI. Do adenocarcinomas of the prostate with Gleason score (GS) </=6 have the potential to metastasize to lymph nodes? Am J Surg Pathol 2012;36:1346-52.
94. Eggener SE, Scardino PT, Walsh PC, Han M, Partin AW, Trock BJ, et al. Predicting 15-year prostate cancer specific mortality after radical prostatectomy. J Urol 2011;185:869-75.
95. Haffner MC, Mosbruger T, Esopi DM, Fedor H, Heaphy CM, Walker DA, et al. Tracking the clonal origin of lethal prostate cancer. J Clin Invest 2013;123:4918-22.
96. Amis ES, Jr., Bigongiari LR, Bluth EI, Bush WH, Jr., Choyke PL, Fritzsche P, et al. Pretreatment staging of clinically localized prostate cancer. American College of Radiology. ACR Appropriateness Criteria. Radiology 2000;215 Suppl:703-8.
97. Greene KL, Albertsen PC, Babaian RJ, Carter HB, Gann PH, Han M, et al. Prostate specific antigen best practice statement: 2009 update. J Urol 2009;182:2232-41.
98. Heidenreich A, Aus G, Bolla M, Joniau S, Matveev VB, Schmid HP, et al. EAU guidelines on prostate cancer. Eur Urol 2008;53:68-80.
99. Mohler J, Bahnson RR, Boston B, Busby JE, D'Amico A, Eastham JA, et al. NCCN clinical practice guidelines in oncology: prostate cancer. J Natl Compr Canc Netw 2010;8:162-200.
100. Lavery HJ, Brajtbord JS, Levinson AW, Nabizada-Pace F, Pollard ME, Samadi DB. Unnecessary imaging for the staging of low-risk prostate cancer is common. Urology 2011;77:274-8.
101. Wolters T, Roobol MJ, van Leeuwen PJ, van den Bergh RC, Hoedemaeker RF, van Leenders GJ, et al. A critical analysis of the tumor volume threshold for clinically insignificant prostate cancer using a data set of a randomized screening trial. J Urol 2011;185:121-5.
102. Klotz L, Zhang L, Lam A, Nam R, Mamedov A, Loblaw A. Clinical results of long-term follow-up of a large, active surveillance cohort with localized prostate cancer. J Clin Oncol 2010;28:126-31.
103. Popiolek M, Rider JR, Andren O, Andersson SO, Holmberg L, Adami HO, et al. Natural history of early, localized prostate cancer: a final report from three decades of follow-up. Eur Urol 2013;63:428-35.
104. Ayers F, Grant A, Kuo D, Cuccia DJ, Durkin AJ. Fabrication and

characterization of silicone-based tissue phantoms with tunable optical properties in the visible and near infrared domain. Biomedical Optics (BiOS) 2008: International Society for Optics and Photonics; 2008. p.687007--9.
105. Ahmed HU, Hindley RG, Dickinson L, Freeman A, Kirkham AP, Sahu M, et al. Focal therapy for localised unifocal and multifocal prostate cancer: a prospective development study. Lancet Oncol 2012;13:622-32.
106. Valerio M, Ahmed HU, Emberton M, Lawrentschuk N, Lazzeri M, Montironi R, et al. The Role of Focal Therapy in the Management of Localised Prostate Cancer: A Systematic Review. Eur Urol 2013.
107. Dall'Era MA, Konety BR, Cowan JE, Shinohara K, Stauf F, Cooperberg MR, et al. Active surveillance for the management of prostate cancer in a contemporary cohort. Cancer 2008;112:2664-70.
108. Cooperberg MR, Broering JM, Carroll PR. Time trends and local variation in primary treatment of localized prostate cancer. J Clin Oncol 2010;28:1117-23.
109. D'Amico AV, Whittington R, Malkowicz SB, Schultz D, Blank K, Broderick GA, et al. Biochemical outcome after radical prostatectomy, external beam radiation therapy, or interstitial radiation therapy for clinically localized prostate cancer. JAMA 1998;280:969-74.
110. Thompson I, Thrasher JB, Aus G, Burnett AL, Canby-Hagino ED, Cookson MS, et al. Guideline for the management of clinically localized prostate cancer: 2007 update. J Urol 2007;177:2106-31.
111. Roach M, Lu J, Pilepich MV, Asbell SO, Mohiuddin M, Terry R, et al. Four prognostic groups predict long-term survival from prostate cancer following radiotherapy alone on Radiation Therapy Oncology Group clinical trials. Int J Radiat Oncol Biol Phys 2000;47:609-15.
112. Cooperberg MR, Pasta DJ, Elkin EP, Litwin MS, Latini DM, Du Chane J, et al. The University of California, San Francisco Cancer of the Prostate Risk Assessment score: a straightforward and reliable preoperative predictor of disease recurrence after radical prostatectomy. J Urol 2005;173:1938-42.
113. Huang J, Vicini FA, Williams SG, Ye H, McGrath S, Ghilezan M, et al. Percentage of positive biopsy cores: a better risk stratification model for prostate cancer? Int J Radiat Oncol Biol Phys 2012;83:1141-8.
114. Chang AJ, Autio KA, Roach M, 3rd, Scher HI. High-risk prostate cancer-classification and therapy. Nat Rev Clin Oncol 2014;11:308-23.
115. Bolla M, Collette L, Blank L, Warde P, Dubois JB, Mirimanoff RO, et al. Long-term results with immediate androgen suppression and external irradiation in patients with locally advanced prostate cancer (an EORTC study): a phase III randomised trial. Lancet

2002;360:103-6.
116. Pilepich MV, Winter K, Lawton CA, Krisch RE, Wolkov HB, Movsas B, et al. Androgen suppression adjuvant to definitive radiotherapy in prostate carcinoma--long-term results of phase III RTOG 85-31. Int J Radiat Oncol Biol Phys 2005;61:1285-90.
117. Widmark A, Klepp O, Solberg A, Damber JE, Angelsen A, Fransson P, et al. Endocrine treatment, with or without radiotherapy, in locally advanced prostate cancer (SPCG-7/SFUO-3): an open randomised phase III trial. Lancet 2009;373:301-8.
118. Warde P, Mason M, Ding K, Kirkbride P, Brundage M, Cowan R, et al. Combined androgen deprivation therapy and radiation therapy for locally advanced prostate cancer: a randomised, phase 3 trial. Lancet 2011;378:2104-11.
119. Petrelli F, Vavassori I, Coinu A, Borgonovo K, Sarti E, Barni S. Radical Prostatectomy or Radiotherapy in High-Risk Prostate Cancer: A Systematic Review and Metaanalysis. Clin Genitourin Cancer 2014.
120. Valicenti RK, Thompson I, Jr., Albertsen P, Davis BJ, Goldenberg SL, Wolf JS, et al. Adjuvant and salvage radiation therapy after prostatectomy: American Society for Radiation Oncology/American Urological Association guidelines. Int J Radiat Oncol Biol Phys 2013;86:822-8.
121. Thompson IM, Valicenti RK, Albertsen P, Davis BJ, Goldenberg SL, Hahn C, et al. Adjuvant and salvage radiotherapy after prostatectomy: AUA/ASTRO Guideline. J Urol 2013;190:441-9.
122. Heidenreich A, Bellmunt J, Bolla M, Joniau S, Mason M, Matveev V, et al. EAU guidelines on prostate cancer. Part 1: screening, diagnosis, and treatment of clinically localised disease. Eur Urol 2011;59:61-71.
123. Sun M, Sammon JD, Becker A, Roghmann F, Tian Z, Kim SP, et al. Radical prostatectomy vs radiotherapy vs observation among older patients with clinically localized prostate cancer: a comparative effectiveness evaluation. BJU Int 2014;113:200-8.
124. Gomella LG, Petrylak DP, Shayegan B. Current management of advanced and castration resistant prostate cancer. Can J Urol 2014;21:1-6.
125. Thoreson GR, Gayed BA, Chung PH, Raj GV. Emerging therapies in castration resistant prostate cancer. Can J Urol 2014;21:98-105.
126. Rove KO, Crawford ED. Traditional androgen ablation approaches to advanced prostate cancer: new insights. Can J Urol 2014;21:14-21.
127. Moul JW. Utility of LHRH antagonists for advanced prostate cancer. Can J Urol 2014;21:22-7.
128. Small EJ, Vogelzang NJ. Second-line hormonal therapy for advanced prostate cancer: a shifting paradigm. J Clin Oncol 1997;15:382-8.
129. Al-Asaaed S, Winquist E. Secondary hormonal manipulation in

castration resistant prostate cancer. Can J Urol 2014;21:37-41.
130. Simpson CR, Kohl M, Essenpreis M, Cope M. Near-infrared optical properties of ex vivo human skin and subcutaneous tissues measured using the Monte Carlo inversion technique. Phys Med Biol 1998;43:2465-78.
131. Svensson T, Andersson-Engels S, Einarsdottir M, Svanberg K. In vivo optical characterization of human prostate tissue using near-infrared time-resolved spectroscopy. J Biomed Opt 2007;12:014022.
132. Zhu TC, Dimofte A, Finlay JC, Stripp D, Busch T, Miles J, et al. Optical properties of human prostate at 732 nm measured in mediated photodynamic therapy. Photochem Photobiol 2005;81:96-105.
133. Sandell JL, Zhu TC. A review of in-vivo optical properties of human tissues and its impact on PDT. J Biophotonics 2011;4:773-87.
134. Dehghani H, Eames ME, Yalavarthy PK, Davis SC, Srinivasan S, Carpenter CM, et al. Near infrared optical tomography using NIRFAST: Algorithm for numerical model and image reconstruction. Communications in numerical methods in engineering 2009;25:711-32.
135. Jermyn M, Ghadyani H, Mastanduno MA, Turner W, Davis SC, Dehghani H, et al. Fast segmentation and high-quality three-dimensional volume mesh creation from medical images for diffuse optical tomography. Journal of biomedical optics 2013;18:086007-.

ABSTRACT(IN KOREAN)

국소 전립선암의 위치결정 정확도 향상을 위한 다채널 근적외선분광 시스템

<지도교수 정대철>

연세대학교 대학원 의학과

김승섭

목적: 국소 전립선암의 위치결정을 위한 영상 진단의 정확도 향상을 위해 다채널 근적외선분광 시스템을 개발하고, 전립선암 광학 팬텀 연구를 통하여 그 정확도를 평가한다.

대상과 방법: 다채널 근적외선분광 시스템을 개발하였고, Labview 프로그래밍 (National Instruments, Austin, TX, USA)을 이용하여 획득신호 처리와 신호변화의 실시간 모니터링을 위한 GUI (Graphic User Interface)를 구성하였다. 정상 전립선과 국소 전립선암의 광학 팬텀을 제작하고, 개발한 근적외선분광 시스템을 적용하여 광학 신호를 검출한 후, 신호분석을 통한 단면 영상 재구성을 수행하였다. 광학 팬텀의 국소전립선암 모델의 실제 위치와 재구성 신호를 비교하여 그 정확도를 분석하였다.

결과: 재구성한 단면 영상에서 높은 흡수 계수를 보였던 구역은 광학 팬텀의 국소전립선암 모델의 실제 위치와 잘 일치하였다.

결론: 다채널 근적외선분광 영상 시스템으로 국소 전립선암의 전립선내 위치결정의 정확도를 높일 수 있는 가능성을 팬텀 연구를 통하여 보여주었다. 이는 향후 기존의 실시간 초음파영상과 융합하여 전립선암의 영상진단의 정확도를 높이고 생검 위치 결정의 정확도를 높이는 새로운 영상기법으로 이용될 수 있을 것이다.

핵심되는 말 : 전립선암, 근적외선분광, 근적외선, 광학 영상, 광학, 근적외선분광-초음파, 융합 영상